Spin-mixing conductances of thin magnetic films from first principles

K. Carva[1,*] and I. Turek[2,†]

[1]*Department of Condensed Matter Physics, Charles University, Faculty of Mathematics and Physics, Ke Karlovu 5, CZ-12116 Prague 2, Czech Republic*

[2]*Institute of Physics of Materials, Academy of Sciences of the Czech Republic, Žižkova 22, CZ-61662 Brno, Czech Republic*

(Received 23 April 2007; revised manuscript received 30 July 2007; published 10 September 2007)

We present a first-principles theory of the spin-mixing conductance for a thin ferromagnetic film embedded epitaxially between two nonmagnetic metallic electrodes. The complex spin-mixing conductance is formulated as a linear response of the spin torque experienced by the film due to the spin accumulation in one of the electrodes. The derivation is based on nonequilibrium Green's functions; the obtained result for the torque response is in agreement with the response of spin fluxes on both sides of the ferromagnet as well as with expressions derived within the Landauer-Büttiker scattering theory. Numerical implementation of the developed formalism employs the tight-binding linear muffin-tin orbital method and calculations are performed for selected metallic and half-metallic ferromagnetic films relevant for spintronics applications. The spin-mixing conductance of the Cu/Ni/Cu(100) system is found to exhibit pronounced oscillations as a function of Ni thickness; their period is explained by spin-resolved Fermi-surface properties of nickel. Investigated half-metallic films include the full-Heusler Co_2MnSi compound and the diluted (Ga,Mn)As magnetic semiconductors attached to nonmagnetic Cr(100) leads; the imaginary part of their spin-mixing conductance has a magnitude comparable to the real part. This unusual feature has been qualitatively explained in terms of a free-electron model.

DOI: 10.1103/PhysRevB.76.104409 PACS number(s): 75.70.−i, 72.10.Bg, 72.25.Pn, 85.75.−d

I. INTRODUCTION

Artificially prepared metallic magnetic multilayers and spin valves attract ongoing interest due to a unique interplay between their magnetic structure and transport properties,[1,2] especially in the current perpendicular to the planes (CPP) geometry. This can be documented by the well-known giant magnetoresistance (GMR) effect[3] and by a more recent prediction[4,5] and realization[6] of the current-induced magnetization switching (CIMS). Subsequent research activities resulted, e.g., in a full control of the sign of both GMR and CIMS in spin valves containing two ferromagnetic layers separated by a nonmagnetic metal[7] or in a significant reduction of the critical current density necessary for CIMS as achieved in tunnel junctions containing a diluted ferromagnetic semiconductor.[8]

The most successful phenomenological framework for quantitative understanding of both phenomena is the Valet-Fert model[9] based on the linearized Boltzmann equation with a collision term accounting for the spin-flip scattering. The latter mechanism provides an extension of the widely used two-current series-resistor model[3] and it has important consequences for layer thicknesses comparable to the so-called spin-diffusion length. The description of the CPP transport in collinear spin structures within this scheme leads to a semiclassical concept of the spin accumulation in nonmagnetic layers, i.e., to a difference of effective chemical potentials (Fermi levels) for electrons in the two spin channels.

A recent generalization of the Valet-Fert model to noncollinear spin structures[10–12] rests heavily on two additional properties of spin currents. First, the transverse (perpendicular to local exchange field) component of the spin current inside a ferromagnet becomes rapidly damped over a typical distance of a few interatomic spacings.[13,14] This very short magnetic coherence length is a result of a large exchange splitting which leads to mostly destructive interference effects due to all contributions of wave vectors on the two Fermi surfaces of the ferromagnetic metal. Consequently, the spin torque experienced by a ferromagnetic (FM) layer can be identified with the transverse spin current at its interface with a neighboring nonmagnetic (NM) layer. Second, the proper boundary conditions inevitable for a full solution of the diffusion equations must be formulated in terms of spin-mixing conductances of individual interfaces.[15] The latter (complex) quantities together with the spin-resolved interface conductances provide a complete information on a linear response of the currents and spin currents at an interface due to the bias and spin accumulation deep inside the neighboring materials.

The magnetoelectronic circuit theory[15–17] represents another flexible approach to the transport properties of noncollinear magnetic systems consisting of FM and NM elements (nodes). This scheme is highly efficient especially when dimensions of individual nodes are smaller than the spin-diffusion lengths but bigger than the electron mean-free paths of the corresponding materials. Within the developed formalism, the chemical potentials and spin accumulations of the nodes are contained in 2×2 distribution matrices in the spin space while junctions among the nodes are featured by the spin-resolved and spin-mixing conductances. The steady-state currents, spin currents, and spin torques in a device can be obtained from applied voltages by solving a set of linear equations quite similar to Kirchhoff's laws for usual electronic circuits, see Ref. 17 for a review.

A truly microscopic (quantum mechanical) approach to all aspects of the GMR and CIMS seems to be prohibitively complicated having in mind the large layer thicknesses and the quality of interfaces in presently used multilayers and spin valves. A reasonable compromise between the accuracy

and the complexity has been adopted by several authors in addressing the spin-polarized electronic and transport properties of a single FM/NM interface[13,18] with emphasis put on the conductances and their sensitivity, e.g., to interface alloying. Since the traditional scheme for the transport, namely, the Landauer-Büttiker scattering theory,[17,19] has been used in majority of papers, the effect of disorder was included by a supercell technique.[17,20]

The spin-mixing conductances of FM films of a finite thickness attached to two NM leads have been studied very recently for Co/Cu, Fe/Au, and Fe/Cr systems.[17,21] It has been found that the thickness dependence of the real part of the spin-mixing conductance saturates very rapidly for thicker films and that its value can be well approximated by the Sharvin conductance of the NM electrode. This behavior is equivalent to the very short magnetic coherence length and it proves that the spin-mixing conductance is predominantly an interface property. However, as suggested by several authors, this may not hold for other ferromagnets such as Ni (Ref. 13) or the diluted magnetic semiconductors (Ga,Mn)As,[11] where the average exchange splitting is much smaller than in the 3*d* transition metals and the size of the Fermi surface is small which could enhance the coherence length.[17]

For systems investigated so far, the imaginary part of the spin-mixing conductance was found to be much smaller than the real part.[18,21] This feature is closely linked to properties of the current-induced steady-state torques in noncollinear spin valves and it results in a very small torque component perpendicular to the plane spanned by magnetization directions of the two FM layers.[12] The assumption of a negligible imaginary part of the spin-mixing conductance has also been employed in theoretical studies of angular magnetoresistance of spin valves[22] as well as of magnetization dynamics of thin FM films;[21] its validity, however, has to be checked in each particular case. As indicated by several authors, this becomes especially important for nonmetallic systems, such as systems containing tunneling barriers[18] or insulating FM parts.[23]

The purpose of the present paper is threefold. First, we consider a FM film embedded between two NM metallic leads with epitaxial interfaces and give a general theoretical formulation of the spin torque and the spin fluxes due to the spin accumulation in one of the electrodes (Sec. II). We use the language of nonequilibrium Green's functions[19,24] (NGF) which in the present context is equivalent to the Landauer-Büttiker theory but it yields formulas that can be more easily evaluated by means of standard Green's-function techniques. Second, we describe briefly a numerical implementation within the first-principles tight-binding linear muffin-tin orbital (TB-LMTO) method[25,26] (Sec. III). The method has recently been combined with the coherent potential approximation[26–29] (CPA) for charge CPP transport in disordered multilayers[30] and we employ the CPA here as well. Finally, we perform calculations and discuss the results for a model Cu/Ni/Cu(100) system followed by a study of more complex magnetic films with potential applicability in spintronics: a binary random alloy $Ni_{0.84}Fe_{0.16}$ (Permalloy, Py), the half-metallic ferromagnet Co_2MnSi, and the diluted magnetic semiconductor (Ga,Mn)As (Sec. IV).

II. THEORY

A. Response of the spin torque

We consider a NM/FM/NM system with noninteracting electrons. Its effective one-electron Hamiltonian H can be written as

$$H = H_0 + \gamma(\boldsymbol{\sigma}\cdot\mathbf{n}), \tag{1}$$

where H_0 represents a spin-independent part, γ is the exchange splitting which is nonzero only inside an intermediate region containing the FM film and narrow parts of the two adjacent semi-infinite NM leads, the vector $\boldsymbol{\sigma}=(\sigma_x,\sigma_y,\sigma_z)$ denotes a vector of the Pauli matrices, and the unit vector $\mathbf{n}$ defines the direction of the exchange field of the FM film. The spin dependence of the Hamiltonian H in Eq. (1) implies that electrons with spin parallel and antiparallel to $\mathbf{n}$ experience Hamiltonians $H_\uparrow=H_0+\gamma$ and $H_\downarrow=H_0-\gamma$, respectively.

We define the spin torque $\boldsymbol{\tau}$ as the time derivative of the total spin magnetic moment. The latter operator is represented by the Pauli matrices $\boldsymbol{\sigma}$, so that

$$\boldsymbol{\tau} = -i[\boldsymbol{\sigma},H], \tag{2}$$

where atomic units ($\hbar=1$) are used. This definition of the spin torque differs formally from the usual definition based on the spin currents on both sides of the FM film;[4,31] equivalence of both approaches for spin valves has been given by a number of authors[32,33] while their equivalence in the present case is proved in Sec. II B. The well-known algebraic rules for the Pauli matrices

$$(\boldsymbol{\sigma}\cdot\mathbf{p})(\boldsymbol{\sigma}\cdot\mathbf{q}) = \mathbf{p}\cdot\mathbf{q} + i(\mathbf{p}\times\mathbf{q})\cdot\boldsymbol{\sigma},$$

$$(\boldsymbol{\sigma}\cdot\mathbf{p})\boldsymbol{\sigma} = \mathbf{p} + i\boldsymbol{\sigma}\times\mathbf{p}, \tag{3}$$

$$\boldsymbol{\sigma}(\boldsymbol{\sigma}\cdot\mathbf{q}) = \mathbf{q} + i\mathbf{q}\times\boldsymbol{\sigma},$$

valid for arbitrary classical vectors $\mathbf{p}$ and $\mathbf{q}$, yield an explicit form of the torque operator

$$\boldsymbol{\tau} = 2\gamma\mathbf{n}\times\boldsymbol{\sigma}. \tag{4}$$

This relation shows that the spin torque is a local operator nonzero only inside the intermediate region with a direction perpendicular to the exchange field of the FM film.

The thermodynamic average of the spin torque $\boldsymbol{\tau}$ for the NM/FM/NM system in a stationary nonequilibrium state is given by

$$\bar{\boldsymbol{\tau}} = \frac{1}{2\pi}\int_{-\infty}^{\infty} \mathrm{Tr}\{\boldsymbol{\tau}G^<(E)\}dE, \tag{5}$$

where $G^<(E)$ is the lesser component of the NGF.[19,24] The latter quantity is related to the retarded and advanced Green's functions $G^r(E)$ and $G^a(E)$ by means of[34]

$$G^<(E) = G^r(E)\Sigma^<(E)G^a(E),$$

$$G^r(E) = [E - H - \Sigma^r(E)]^{-1}, \tag{6}$$

$$G^a(E) = [E - H - \Sigma^a(E)]^{-1},$$

where $\Sigma^<(E)$, $\Sigma^r(E)$, and $\Sigma^a(E)$ denote the lesser, retarded, and advanced components of the self-energy, respectively. Note that all operators in Eqs. (5) and (6) are defined in the Hilbert space of the intermediate region.

The spin accumulation in the NM leads results in a change of the lesser self-energy $\delta\Sigma^<(E)$ (see below) which induces the following first-order change of the thermodynamic average (5):

$$\delta\tilde{\boldsymbol{\tau}} = \frac{1}{2\pi}\int_{-\infty}^{\infty} \mathrm{Tr}\{G^a(E)\boldsymbol{\tau}G^r(E)\delta\Sigma^<(E)\}dE. \tag{7}$$

The special form of the torque operator, Eq. (2), together with the expression for $G^{r,a}(E)$, Eq. (6), provide a relation

$$G^a(E)\boldsymbol{\tau}G^r(E) = -i[\boldsymbol{\sigma}G^r(E) - G^a(E)\boldsymbol{\sigma}] + G^a(E)\boldsymbol{\sigma}\Gamma(E)G^r(E), \tag{8}$$

where we introduced the usual abbreviation for the anti-Hermitean part of the self-energy, namely,

$$\Gamma(E) = i[\Sigma^r(E) - \Sigma^a(E)]. \tag{9}$$

In deriving Eq. (8), use was made of the fact that the self-energies of the unperturbed NM leads are spin independent, hence $[\boldsymbol{\sigma}, \Sigma^{r,a}(E)]=0$.

The total self-energies can be written as sums of separate contributions due to the left ($\mathcal{L}$) and the right ($\mathcal{R}$) leads,

$$\Sigma^x(E) = \Sigma^x_{\mathcal{L}}(E) + \Sigma^x_{\mathcal{R}}(E), \quad x = r, a, <. \tag{10}$$

For stationary nonequilibrium systems without spin accumulation, the lesser self-energies are given by

$$\Sigma^<_{\mathcal{L},\mathcal{R}}(E) = f_{\mathcal{L},\mathcal{R}}(E)\Gamma_{\mathcal{L},\mathcal{R}}(E),$$
$$\Gamma_{\mathcal{L},\mathcal{R}}(E) = i[\Sigma^r_{\mathcal{L},\mathcal{R}}(E) - \Sigma^a_{\mathcal{L},\mathcal{R}}(E)], \tag{11}$$

where the functions $f_{\mathcal{L},\mathcal{R}}(E)$ refer to the Fermi-Dirac distributions of the two leads. Note that $\Gamma(E)=\Gamma_{\mathcal{L}}(E)+\Gamma_{\mathcal{R}}(E)$.

In the thermodynamic equilibrium, the distributions $f_{\mathcal{L},\mathcal{R}}(E)$ coincide with the Fermi-Dirac distribution of the whole system. In the presence of spin accumulation in one of the leads ($\mathcal{L}$), the system is driven out of equilibrium by adding a spin-dependent shift to the Fermi energy of the lead characterized by a magnitude $\delta E_{\mathcal{L}}$. This yields the first-order change of the lesser self-energy in a form

$$\delta\Sigma^<(E) = \delta\Sigma^<_{\mathcal{L}}(E) = f'(E)(\boldsymbol{\sigma}\cdot\mathbf{a})\Gamma_{\mathcal{L}}(E)\delta E_{\mathcal{L}}, \tag{12}$$

where $f'(E)$ means the derivative of the Fermi-Dirac distribution and $\mathbf{a}$ is a unit vector pointing in the direction of spin accumulation. The spin-dependent $\delta\Sigma^<(E)$ according to Eq. (12) describes compactly a change of the left-lead Fermi energy by $-\delta E_{\mathcal{L}}$ ($+\delta E_{\mathcal{L}}$) for electrons with spin parallel (antiparallel) to the spin accumulation direction $\mathbf{a}$. For systems at zero temperature, which will be considered in the following, $f'(E)=-\delta(E-E_F)$ where E_F is the Fermi energy. Substitution of Eqs. (8) and (12) into Eq. (7) provides a starting expression for the corresponding response coefficient $\mathbf{C}_{\mathcal{L}}$:

$$\mathbf{C}_{\mathcal{L}} \equiv \frac{\delta\tilde{\boldsymbol{\tau}}}{\delta E_{\mathcal{L}}} = \frac{1}{2\pi}\mathrm{Tr}[i(\boldsymbol{\sigma}G^r - G^a\boldsymbol{\sigma})(\boldsymbol{\sigma}\cdot\mathbf{a})\Gamma_{\mathcal{L}} - \boldsymbol{\sigma}\Gamma G^r(\boldsymbol{\sigma}\cdot\mathbf{a})\Gamma_{\mathcal{L}}G^a], \tag{13}$$

where all omitted energy arguments equal the Fermi energy E_F.

In order to extract the dependence of the response coefficient $\mathbf{C}_{\mathcal{L}}$ on orientation of the spin accumulation $\mathbf{a}$ and the magnetization direction $\mathbf{n}$, the explicit structure of the Green's functions $G^{r,a}$ of the Hamiltonian (1) with respect to the spin must be used,

$$G^{r,a} = \frac{G^{r,a}_{\uparrow} + G^{r,a}_{\downarrow}}{2} + \frac{G^{r,a}_{\uparrow} - G^{r,a}_{\downarrow}}{2}(\boldsymbol{\sigma}\cdot\mathbf{n}), \tag{14}$$

where the spin-resolved Green's functions are defined by

$$G^{r,a}_s(E) = [E - H_s - \Sigma^{r,a}(E)]^{-1}, \quad s = \uparrow, \downarrow. \tag{15}$$

The substitution of Eq. (14) into Eq. (13) reduces its r.h.s. to a sum of terms of the form $\mathrm{Tr}(\xi X)=\mathrm{tr}_S(\xi)\mathrm{tr}(X)$, where ξ is a matrix in the spin indices only while X is a matrix in the other (site and orbital) indices and where the symbols tr_S and tr denote the respective trace operations. Further steps employ the rules (3) and their consequences for trace relations:

$$\mathrm{tr}_S[\boldsymbol{\sigma}(\boldsymbol{\sigma}\cdot\mathbf{a})] = 2\mathbf{a},$$
$$\mathrm{tr}_S[\boldsymbol{\sigma}(\boldsymbol{\sigma}\cdot\mathbf{n})(\boldsymbol{\sigma}\cdot\mathbf{a})] = 2i\mathbf{n}\times\mathbf{a}, \tag{16}$$
$$\mathrm{tr}_S[\boldsymbol{\sigma}(\boldsymbol{\sigma}\cdot\mathbf{n})(\boldsymbol{\sigma}\cdot\mathbf{a})(\boldsymbol{\sigma}\cdot\mathbf{n})] = 4(\mathbf{n}\cdot\mathbf{a})\mathbf{n} - 2\mathbf{a}.$$

The resulting expression for $\mathbf{C}_{\mathcal{L}}$ follows after a lengthy but straightforward manipulation:

$$\mathbf{C}_{\mathcal{L}} = D_1\mathbf{a} + D_2\mathbf{a}\times\mathbf{n} - D_3(\mathbf{n}\cdot\mathbf{a})\mathbf{n}, \tag{17}$$

where the prefactors D_1, D_2, and D_3 are given by

$$D_1 = \frac{1}{2\pi}\mathrm{tr}[i(G^r_{\uparrow} + G^r_{\downarrow} - G^a_{\uparrow} - G^a_{\downarrow})\Gamma_{\mathcal{L}} - \Gamma G^r_{\uparrow}\Gamma_{\mathcal{L}}G^a_{\downarrow} - \Gamma G^r_{\downarrow}\Gamma_{\mathcal{L}}G^a_{\uparrow}],$$

$$D_2 = \frac{1}{2\pi}\mathrm{tr}[(G^r_{\uparrow} - G^r_{\downarrow} + G^a_{\uparrow} - G^a_{\downarrow})\Gamma_{\mathcal{L}} + i(\Gamma G^r_{\uparrow}\Gamma_{\mathcal{L}}G^a_{\downarrow} - \Gamma G^r_{\downarrow}\Gamma_{\mathcal{L}}G^a_{\uparrow})], \tag{18}$$

$$D_3 = \frac{1}{2\pi}\mathrm{tr}[\Gamma(G^r_{\uparrow} - G^r_{\downarrow})\Gamma_{\mathcal{L}}(G^a_{\uparrow} - G^a_{\downarrow})].$$

The form of Eq. (17) can be simplified by using a general relation

$$i[G^r(E) - G^a(E)] = G^a(E)\Gamma(E)G^r(E) \tag{19}$$

that follows from Eqs. (6) and (9). After inserting the spin-resolved counterparts of Eq. (19), $i(G^r_s - G^a_s) = G^a_s\Gamma G^r_s$ ($s=\uparrow,\downarrow$), in the expression (18) for D_1 one obtains $D_3=D_1$. The previous formula (17) for the response coefficient $\mathbf{C}_{\mathcal{L}}$ can thus be rewritten in a form of a vector explicitly perpendicular to the vector $\mathbf{n}$:

$$\mathbf{C}_{\mathcal{L}} = D_1 \mathbf{n} \times (\mathbf{a} \times \mathbf{n}) + D_2 \mathbf{a} \times \mathbf{n}. \tag{20}$$

The first term in $\mathbf{C}_{\mathcal{L}}$ refers to the torque component lying in the plane containing the two vectors $\mathbf{n}$ and $\mathbf{a}$ (in-plane component), while the second term refers to the component perpendicular to this plane (out-of-plane component). A closer inspection of the real quantities D_1 and D_2, Eq. (18), reveals their simple relation to a single complex quantity—the spin-mixing conductance $C_{\mathcal{L}}^{\mathrm{mix}}$:

$$C_{\mathcal{L}}^{\mathrm{mix}} = \frac{1}{2\pi} \mathrm{tr}[i(G_{\uparrow}^{r} - G_{\downarrow}^{a})\Gamma_{\mathcal{L}} - \Gamma G_{\uparrow}^{r} \Gamma_{\mathcal{L}} G_{\downarrow}^{a}], \tag{21}$$

which yields

$$D_1 = 2\ \mathrm{Re}\ C_{\mathcal{L}}^{\mathrm{mix}}, \quad D_2 = 2\ \mathrm{Im}\ C_{\mathcal{L}}^{\mathrm{mix}}. \tag{22}$$

Note that the complex response coefficient $C_{\mathcal{L}}^{\mathrm{mix}}$ is sometimes denoted as a "spin-pumping conductance."[21,35] The formulas (20)–(22) represent the central result of this section.

The real part of the $C_{\mathcal{L}}^{\mathrm{mix}}$ is always positive, as can be shown from the identity $D_1 = D_3$, see Eq. (18) and the text below Eq. (19), and from the positive definiteness of the operators $\Gamma_{\mathcal{L},\mathcal{R}}$. Consequently, the in-plane torque component is always positive and the spin accumulation tends to align the magnetization direction $\mathbf{n}$ toward the spin accumulation direction $\mathbf{a}$. A recent theoretical study of Co/Cu/Co(111) structures has predicted that the in-plane torque due to an applied spin-independent bias can change its sign with varying thickness of the Co layer.[32] This qualitative difference indicates that the phase coherence across a structure containing two noncollinear magnetic layers gives rise to a more complex behavior than that due to noncollinearity between the semiclassical spin accumulation and the exchange splitting of a single FM film. Another interesting change of the sign of the in-plane torque component has been predicted for magnetic tunnel junctions under a sufficiently high bias.[36] A direct comparison of this phenomenon to results of the present linear-response theory seems to be impossible; moreover, the necessary high bias values can hardly be realized in metallic systems studied here.

B. Relation to spin currents

It is well known that spin torques acting on FM layers of a magnetic multilayer are closely related to spin currents flowing through the structure. The physical origin of this relation can be traced back to a general theorem for the time derivative of the spin (magnetization) density of a many-electron system which can be expressed by means of the divergence of the spin-current tensor and the spin-torque density.[13,37] Application of this theorem to stationary states gives the spin torque acting on an arbitrary spatial region exactly equal to the flux of the spin current across the surface of the region, i.e., equal to the surface integral of the spin-current tensor. In the present case, the spatial region comprises naturally the FM film and a few neighboring atomic layers on its both sides; its surface is formed by two boundary planes parallel to the film and located outside it. The spin fluxes on the two sides of the FM film are defined as

$$\begin{aligned} \mathbf{J}_{\mathcal{L}} &= -i\boldsymbol{\sigma}[\Pi_{\mathcal{L}}, H_0] = -i[\boldsymbol{\sigma}\Pi_{\mathcal{L}}, H], \\ \mathbf{J}_{\mathcal{R}} &= -i\boldsymbol{\sigma}[\Pi_{\mathcal{R}}, H_0] = -i[\boldsymbol{\sigma}\Pi_{\mathcal{R}}, H], \end{aligned} \tag{23}$$

where the kinetic energy (intersite hopping) is contained in the spin-independent part H_0 of the Hamiltonian H, Eq. (1), and where the $\Pi_{\mathcal{L}}$ and $\Pi_{\mathcal{R}}$ denote projection operators on the respective leads including a few adjacent NM atomic layers of the intermediate region such that $\Pi_{\mathcal{L}}\gamma = \Pi_{\mathcal{R}}\gamma = 0$. Note that the projector operators $\Pi_{\mathcal{L}}$ and $\Pi_{\mathcal{R}}$ project on semi-infinite regions with zero exchange splitting and that the operators $-i[\Pi_{\mathcal{L}}, H_0]$ and $-i[\Pi_{\mathcal{R}}, H_0]$ in the definition of the spin fluxes represent the usual particle fluxes across the two boundary planes. The final expression of the $\mathbf{J}_{\mathcal{L},\mathcal{R}}$ in Eq. (23) has a form of the time derivative due to the full Hamiltonian H; this form is a consequence of the special choice of the projection operators $\Pi_{\mathcal{L},\mathcal{R}}$ and it simplifies the subsequent theoretical analysis considerably. In particular, the linear-response coefficients for the spin fluxes, defined as

$$\mathbf{K}_{\mathcal{L}}^{\mathcal{L}} = \frac{\delta \bar{\mathbf{J}}_{\mathcal{L}}}{\delta E_{\mathcal{L}}}, \quad \mathbf{K}_{\mathcal{L}}^{\mathcal{R}} = \frac{\delta \bar{\mathbf{J}}_{\mathcal{R}}}{\delta E_{\mathcal{L}}}, \tag{24}$$

can be obtained in a similar way as in Sec. II A for the response coefficient $\mathbf{C}_{\mathcal{L}}$, Eq. (13). The explicit expressions are given by

$$\begin{aligned} \mathbf{K}_{\mathcal{L}}^{\mathcal{L}} &= \frac{1}{2\pi} \mathrm{Tr}[i(\boldsymbol{\sigma} G^{r} - G^{a}\boldsymbol{\sigma})(\boldsymbol{\sigma}\cdot\mathbf{a})\Gamma_{\mathcal{L}} - \boldsymbol{\sigma}\Gamma_{\mathcal{L}} G^{r}(\boldsymbol{\sigma}\cdot\mathbf{a})\Gamma_{\mathcal{L}} G^{a}], \\ \mathbf{K}_{\mathcal{L}}^{\mathcal{R}} &= -\frac{1}{2\pi} \mathrm{Tr}[\boldsymbol{\sigma}\Gamma_{\mathcal{R}} G^{r}(\boldsymbol{\sigma}\cdot\mathbf{a})\Gamma_{\mathcal{L}} G^{a}], \end{aligned} \tag{25}$$

where several simple properties of the projectors, such as $[\Pi_{\mathcal{L}}, \Sigma^{r,a}(E)] = 0$ and $\Pi_{\mathcal{L}}\Gamma = \Gamma_{\mathcal{L}}$ (and similarly for $\Pi_{\mathcal{R}}$), were used. Note that $\mathbf{K}_{\mathcal{L}}^{\mathcal{L}} + \mathbf{K}_{\mathcal{L}}^{\mathcal{R}} = \mathbf{C}_{\mathcal{L}}$ which reflects the above mentioned relation between the torque and the spin currents.

The resulting formulas can be summarized as

$$\begin{aligned} \mathbf{K}_{\mathcal{L}}^{\mathcal{L}} &= 2\ \mathrm{Re}\ C_{\mathcal{L}}^{\mathcal{L},\mathrm{mix}} \mathbf{n} \times (\mathbf{a} \times \mathbf{n}) + 2\ \mathrm{Im}\ C_{\mathcal{L}}^{\mathcal{L},\mathrm{mix}} \mathbf{a} \times \mathbf{n} \\ &\quad + (C_{\uparrow} + C_{\downarrow})(\mathbf{n}\cdot\mathbf{a})\mathbf{n}, \\ \mathbf{K}_{\mathcal{L}}^{\mathcal{R}} &= 2\ \mathrm{Re}\ C_{\mathcal{L}}^{\mathcal{R},\mathrm{mix}} \mathbf{n} \times (\mathbf{a} \times \mathbf{n}) + 2\ \mathrm{Im}\ C_{\mathcal{L}}^{\mathcal{R},\mathrm{mix}} \mathbf{a} \times \mathbf{n} \\ &\quad - (C_{\uparrow} + C_{\downarrow})(\mathbf{n}\cdot\mathbf{a})\mathbf{n}, \end{aligned} \tag{26}$$

where we introduced complex coefficients in analogy to the spin-mixing conductance, Eq. (21), namely,

$$\begin{aligned} C_{\mathcal{L}}^{\mathcal{L},\mathrm{mix}} &= \frac{1}{2\pi} \mathrm{tr}[i(G_{\uparrow}^{r} - G_{\downarrow}^{a})\Gamma_{\mathcal{L}} - \Gamma_{\mathcal{L}} G_{\uparrow}^{r} \Gamma_{\mathcal{L}} G_{\downarrow}^{a}], \\ C_{\mathcal{L}}^{\mathcal{R},\mathrm{mix}} &= -\frac{1}{2\pi} \mathrm{tr}(\Gamma_{\mathcal{R}} G_{\uparrow}^{r} \Gamma_{\mathcal{L}} G_{\downarrow}^{a}), \end{aligned} \tag{27}$$

and the spin-resolved charge conductances (in units of $e^2/\hbar$)

$$C_s = \frac{1}{2\pi}\mathrm{tr}(\Gamma_{\mathcal{R}} G_s^r \Gamma_{\mathcal{L}} G_s^a), \quad s = \uparrow, \downarrow. \tag{28}$$

Two comments to these results are now in order. First, the dependence of the spin fluxes on the orientation of the spin accumulation (**a**) and the magnetization (**n**), Eq. (26), is more complicated than that of the spin torque, Eq. (20). Second, an obvious relation $C_{\mathcal{L}}^{\mathrm{mix}} = C_{\mathcal{L}}^{\mathcal{L},\mathrm{mix}} + C_{\mathcal{L}}^{\mathcal{R},\mathrm{mix}}$ can be proved from Eqs. (21) and (27). However, this decomposition does not justify a direct interpretation of the quantities $C_{\mathcal{L}}^{\mathcal{L},\mathrm{mix}}$ and $C_{\mathcal{L}}^{\mathcal{R},\mathrm{mix}}$ as respective contributions to the total spin-mixing conductance due to the left and right spin fluxes, since the latter contain also terms proportional to the total charge conductance $C_\uparrow + C_\downarrow$ and parallel to the magnetization direction **n**, see Eq. (26). Hence, the quantities $C_{\mathcal{L}}^{\mathcal{L},\mathrm{mix}}$ and $C_{\mathcal{L}}^{\mathcal{R},\mathrm{mix}}$ refer only to the transverse components of the left and right spin fluxes with respect to the exchange field of the FM film.

C. Relation to scattering theory

The resulting dependences of the spin torque, Eq. (20), and of the spin fluxes, Eq. (26), on the orientation of the spin accumulation and the magnetization are identical to those obtained within the Landauer-Büttiker scattering theory of transport.[17] In order to make the relation of this traditional tool to the NGF approach more explicit, we consider here the simplest case, namely, a one-dimensional (1D) system with one propagating mode in two identical NM leads.

The configuration space of the system is a real axis with positions denoted by a continuous variable x $(-\infty < x < \infty)$. The spin-independent part of the Hamiltonian is given by $H_0 = -(\partial/\partial x)^2$ (we set the electron mass $m = 1/2$) and the exchange splitting $\gamma(x)$ vanishes for $x \leqslant x_{\mathcal{L}}$ and $x \geqslant x_{\mathcal{R}}$, where the points $x_{\mathcal{L}}$ and $x_{\mathcal{R}}$ denote the boundaries between the NM leads and the intermediate region containing the FM part. The Fermi energy corresponds to a positive kinetic energy in the leads, $E_F = k^2$ with $k > 0$.

The spin-resolved retarded and advanced Green's functions $G_s^{r,a}$ $(s = \uparrow, \downarrow)$ at this real energy are constructed from two independent solutions $\chi_{1s}(x)$ and $\chi_{2s}(x)$ of the Schrödinger equation for the Hamiltonians $H_\uparrow = H_0 + \gamma$ and $H_\downarrow = H_0 - \gamma$. The asymptotics of the two solutions are

$$\begin{aligned} \chi_{1s}(x) &= \exp(ikx) \quad \text{for } x \geqslant x_{\mathcal{R}}, \\ \chi_{2s}(x) &= \exp(-ikx) \quad \text{for } x \leqslant x_{\mathcal{L}}, \end{aligned} \tag{29}$$

and the retarded Green's function is given by

$$\langle x|G_s^r|x'\rangle = W_s^{-1}\chi_{1s}(x_>)\chi_{2s}(x_<), \tag{30}$$

where $W_s = \chi_{2s}(x)[\partial\chi_{1s}(x)/\partial x] - \chi_{1s}(x)[\partial\chi_{2s}(x)/\partial x]$ denotes the (x independent) Wronskian of the two solutions, while $x_> = \max\{x, x'\}$ and $x_< = \min\{x, x'\}$.

The asymptotic behavior of the solution $\chi_{1s}(x)$ for $x \leqslant x_{\mathcal{L}}$ is given by

$$\chi_{1s}(x) = t_s^{-1}[\exp(ikx) + r_s \exp(-ikx)], \tag{31}$$

where we introduced the spin-resolved transmission (t_s) and reflection (r_s) coefficients of the wave incoming from the left. They satisfy the usual condition $|r_s|^2 + |t_s|^2 = 1$ and their knowledge allows us to evaluate explicitly the Wronskian in Eq. (30), $W_s = 2ikt_s^{-1}$, as well as the asymptotics of the solution $\chi_{2s}(x)$ for $x \geqslant x_{\mathcal{R}}$:

$$\chi_{2s}(x) = \frac{1}{t_s}\exp(-ikx) - \frac{r_s^*}{t_s^*}\exp(ikx). \tag{32}$$

These relations yield, e.g., the following elements of the retarded Green's functions:

$$\begin{aligned} \langle x_{\mathcal{L}}|G_s^r|x_{\mathcal{L}}\rangle &= \frac{1}{2ik}[1 + r_s \exp(-2ikx_{\mathcal{L}})], \\ \langle x_{\mathcal{R}}|G_s^r|x_{\mathcal{R}}\rangle &= \frac{1}{2ik}\left[1 - \frac{r_s^* t_s}{t_s^*}\exp(2ikx_{\mathcal{R}})\right], \\ \langle x_{\mathcal{L}}|G_s^r|x_{\mathcal{R}}\rangle &= \frac{t_s}{2ik}\exp[ik(x_{\mathcal{R}} - x_{\mathcal{L}})]. \end{aligned} \tag{33}$$

Other elements, including those of the advanced Green's functions, can be obtained with help of general identities $\langle x'|G_s^r|x\rangle = \langle x|G_s^r|x'\rangle$ and $\langle x|G_s^a|x'\rangle = \langle x|G_s^r|x'\rangle^*$. Since the anti-Hermitean part of the self-energy $\Gamma = \Gamma_{\mathcal{L}} + \Gamma_{\mathcal{R}}$, Eq. (11), is in this particular case given by[38]

$$\begin{aligned} \langle x|\Gamma_{\mathcal{L}}|x'\rangle &= 2k\delta(x - x_{\mathcal{L}})\delta(x' - x_{\mathcal{L}}), \\ \langle x|\Gamma_{\mathcal{R}}|x'\rangle &= 2k\delta(x - x_{\mathcal{R}})\delta(x' - x_{\mathcal{R}}), \end{aligned} \tag{34}$$

the total spin-mixing conductance, Eq. (21), and its left and right contributions due to the transverse spin currents, Eq. (27), are equal to

$$\begin{aligned} C_{\mathcal{L}}^{\mathcal{L},\mathrm{mix}} &= \frac{1}{2\pi}(1 - r_\uparrow r_\downarrow^*), \quad C_{\mathcal{L}}^{\mathcal{R},\mathrm{mix}} = -\frac{1}{2\pi}t_\uparrow t_\downarrow^*, \\ C_{\mathcal{L}}^{\mathrm{mix}} &= \frac{1}{2\pi}(1 - r_\uparrow r_\downarrow^* - t_\uparrow t_\downarrow^*). \end{aligned} \tag{35}$$

Note that the spin-resolved CPP conductances, Eq. (28), reduce within the present model to $C_s = |t_s|^2/(2\pi)$.

The last result, Eq. (35), proves an equivalence of the developed NGF approach to the existing Landauer-Büttiker formalism.[17] In particular, the left contribution $C_{\mathcal{L}}^{\mathcal{L},\mathrm{mix}}$ was identified with the spin-mixing conductance of a single NM/FM interface,[15,16,18] while the transmission term $C_{\mathcal{L}}^{\mathcal{R},\mathrm{mix}}$ appeared naturally for FM films of a finite thickness.[21,22,31,35,39] The presence of several propagating modes in the leads is taken simply into account by double summations over these channels in Eq. (35), see References 16, 17, and 21 for details.

The full equivalence of both approaches has been proven for particle currents due to spin-independent chemical potentials in the leads with any number of propagating channels;[40,41] a similar general proof for spin currents due to the spin accumulation goes beyond the scope of the present paper. In the case of realistic multiorbital tight-binding Hamiltonians, a fundamental question concerns a possible contribution of evanescent states to the transport coefficients. A study of a spinless case[42] indicated that although the evanescent states do not contribute explicitly to the total con-

ductance, their implicit effect has to be taken fully into account, and that an improper treatment can cause serious theoretical flaws, such as a dependence of the calculated flux on the position chosen for its evaluation. While a subsequent paper[43] seems to disprove some of the conclusions of Ref. 42, the most recent studies of the spin-mixing conductance have revealed that evanescent states in FM leads cannot be ignored in accurate calculations of single NM/FM interfaces.[17,21]

We think that detailed assessment of a role of the evanescent states for spin-mixing conductances is less important in the present Green's-function approach; instead, we show in the Appendix that the derived transport coefficients, Eqs. (21) and (27), of the NM/FM/NM systems do not depend on where boundaries between the leads and the intermediate region are chosen. This invariance property represents a most important feature both from a purely theoretical viewpoint and for practical calculations.

III. IMPLEMENTATION

A. Translation into the tight-binding linear muffin-tin orbital method

The *ab initio* TB-LMTO method[25,26,44] proved to be an efficient tool for electronic structure and transport calculations. Various details of this approach for transport properties of bulk and layered systems can be found in the literature both for the Landauer-Büttiker formalism[17,20] and for the Green's-function point of view.[30,45–48] For this reason, we present below only the final TB-LMTO expression for the spin-mixing conductance $C_{\mathcal{L}}^{\mathrm{mix}}$ corresponding to Eq. (21).

The spin-mixing conductance per unit two-dimensional (2D) cell is given by

$$C_{\mathcal{L}}^{\mathrm{mix}} = \frac{1}{2\pi}\frac{1}{N_{\parallel}}\mathrm{tr}[i(g_{\uparrow}^{r} - g_{\downarrow}^{a})\mathcal{B}_{\mathcal{L}} - (\mathcal{B}_{\mathcal{L}} + \mathcal{B}_{\mathcal{R}})g_{\uparrow}^{r}\mathcal{B}_{\mathcal{L}}g_{\downarrow}^{a}], \quad (36)$$

where $N_{\parallel}$ refers to a large number of 2D cells in directions parallel to atomic layers and the trace is taken over the site and orbital indices of the intermediate region. The quantities g_s^r and g_s^a $(s=\uparrow,\downarrow)$ denote spin-resolved auxiliary Green's-function matrices calculated respectively at energies $E_F+i\eta$ and $E_F-i\eta$, where $\eta\to 0^+$. The spin-independent matrices $\mathcal{B}_{\mathcal{L},\mathcal{R}}$ correspond to anti-Hermitean parts of self-energies of the NM leads.[30,45] In the principal-layer technique used here, the intermediate region consists of N principal layers and the $\mathcal{B}_{\mathcal{L}}$ and the $\mathcal{B}_{\mathcal{R}}$ are localized in the first and the Nth principal layer, respectively. Conversion from the atomic units to usual units of conductance is achieved by a prefactor of $e^2/\hbar$ which leads to replacement of $1/(2\pi)$ in Eq. (36) by the conductance quantum e^2/h.

For epitaxial systems with perfect 2D translational symmetry, the evaluation of Eq. (36) rests on the lattice Fourier transformation of the involved matrices. For FM films with substitutional disorder, attached to nonrandom electrodes, the CPA is used for configurational averaging.[26,44] The CPA-vertex corrections due to the second term in Eq. (36) are formulated and calculated according to Ref. 30.

B. Computational details

Details of the self-consistent electronic structure calculations employing the TB-LMTO technique in the atomic sphere approximation (ASA) were described elsewhere;[26,30,44] the present results were based on the local spin-density approximation[49] (LSDA) to the density functional theory[50] with parametrization of the local exchange correlation potential according to Ref. 51 and with a valence basis comprising s, p, and d orbitals. The systems treated in Sec. IV were derived from face-centered-cubic (fcc) and body-centered-cubic (bcc) lattices with neglected lattice relaxations and with layer stacking along the (100) direction; in both cases one principal layer consisted of two neighboring atomic layers.

The energy arguments $E_F \pm i\eta$ for the conductance calculations contained an imaginary part of $\eta = 10^{-7}$ Ry. Evaluation of the trace in Eq. (36) used a uniform mesh in the 2D reciprocal space with densities equivalent to 6400 and 5000 sampling $\mathbf{k}_{\parallel}$ points in the full 2D Brillouin zone (BZ) of the 1×1 unit cell of the attached Cu(100) and Cr(100) leads, respectively.

IV. RESULTS AND DISCUSSION

A. Ni-based magnetic films

The present study of the fcc Cu/Ni/Cu(100) and Cu/Py/Cu(100) systems is performed with a fixed lattice having a lattice parameter between that of pure Ni (0.352 nm) and pure Cu (0.361 nm); the actual value used in the calculations (0.355 nm) is close to the experimental value of a $Ni_{0.80}Fe_{0.20}$ Permalloy.[52] However, the reported results and the conclusions made are qualitatively fairly stable with respect to variations of the lattice parameter within the limits set by pure nickel and copper.

The spin-resolved conductances for the Cu/Ni/Cu(100) system as functions of the Ni thickness are plotted in Fig. 1 (top panel). They exhibit an expected behavior, namely, a nearly constant value for both spin channels with small oscillations due to quantum-size effects. The majority conductance is higher than the minority one due to the well-known spin dependence of the potential difference at the Cu/Ni interface: the majority potentials of both species are nearly identical whereas the minority electrons feel a non-negligible mismatch of the two potentials at the interface. For the same reason, the quantum-size effects are hardly visible in the majority conductance but they are more pronounced in the minority channel. Similar features were found in previous studies of Cu/Ni and Cu/Co based magnetic multilayers;[45,53,54] they are responsible for the CPP-GMR phenomenon.

The real and the imaginary parts of the spin-mixing conductance of the Cu/Ni/Cu(100) system, plotted in Fig. 1 (bottom panel), exhibit a qualitatively different dependence on the Ni thickness as compared to the spin-resolved conductances. The behavior of $C_{\mathcal{L}}^{\mathrm{mix}}$ is characterized by pronounced oscillations with a period of 11 ML (monolayers) and with a large amplitude that decays only slowly with increasing Ni thickness. The observed dependence is also different from the dependences of $C_{\mathcal{L}}^{\mathrm{mix}}$ found for

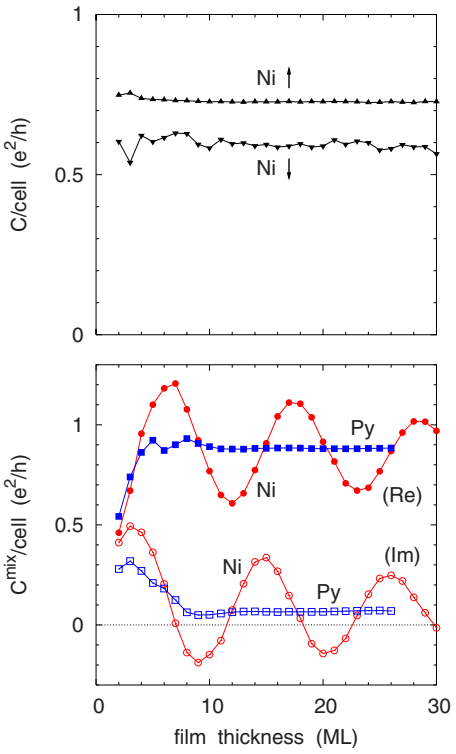

FIG. 1. (Color online) The spin-resolved conductances of Cu/Ni/Cu(100) as functions of the Ni thickness (top panel) and the spin-mixing conductances of Cu/Ni/Cu(100) (red symbols) and Cu/Py/Cu(100) (blue symbols) as functions of the magnetic film thickness (bottom panel). The real and the imaginary parts of the complex spin-mixing conductances are denoted by the full and the empty symbols, respectively.

Cu/Co/Cu(111) and Au/Fe/Au(100) trilayers;[17,21] the oscillations found for the latter systems are smaller in magnitude and they are damped very rapidly being suppressed essentially for magnetic film thicknesses greater than 15 ML. Note that the Re $C_{\mathcal{L}}^{\mathrm{mix}}$ for the Cu/Ni/Cu(100) system oscillates around a mean value that is close to the Sharvin conductance of the fcc Cu(100) lead, $C_{Sh}=0.93e^2/h$ (per one spin and one interface atom), while the mean value of the oscillating Im $C_{\mathcal{L}}^{\mathrm{mix}}$ is appreciably smaller, in qualitative agreement with the other metallic systems.

A quantitative theory of oscillations of the CPP transport properties was formulated a decade ago for the spin-resolved conductances of magnetic multilayers with varying thickness of a NM spacer,[55,56] whereas the case of the spin-mixing conductance of a single magnetic film with varying thickness has been worked out very recently.[17,21] Both approaches emphasize the role of the Fermi-surface (FS) properties of the thick layer, very much in the spirit of the theory of the oscillatory interlayer exchange coupling in magnetic multilayers.[57,58]

In the present case of Cu/Ni/Cu(100), the unimportant oscillations of the conductances in each separate spin channel together with the pronounced oscillations of the spin-mixing conductance (see Fig. 1) indicate that an origin of the latter has to be identified with stationary points of the difference $k_{i\perp}^{\uparrow}-k_{j\perp}^{\downarrow}$ as a function of the $\mathbf{k}_{\parallel}$ point where i and j run

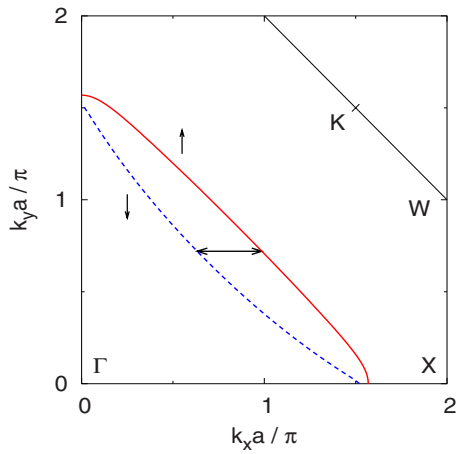

FIG. 2. (Color online) Cross section of the Ni Fermi surfaces for majority (full red curve) and minority (dashed blue curve) spin channels in the (001) plane. The horizontal arrow denotes the position of the $\mathbf{k}_{\parallel}$ vector in the (100) plane corresponding to the stationary point of the difference $k_{\perp}^{\uparrow}-k_{\perp}^{\downarrow}$. The labels Γ, X, W, and K refer to special points of the fcc BZ.

over the individual sheets of the fcc Ni FS in the two spin channels.[17,21]

The majority FS of fcc Ni is rather simple having only a single sheet (topologically similar to the well-known FS of fcc Cu), whereas four sheets are encountered in the minority FS.[59,60] However, one of them, namely, the $e_6^{\downarrow}$ sheet,[59] is nearly parallel to the spin-up FS in large parts of the fcc BZ. The cross sections of these two FS sheets (constructed from the bulk band structure of fcc Ni obtained using the present TB-LMTO-ASA technique) by the plane (001) are shown in Fig. 2. These two sheets give rise to a stationary point of the difference $k_{\perp}^{\uparrow}-k_{\perp}^{\downarrow}$; the corresponding $\mathbf{k}_{\parallel}$ vector and the stationary value of the difference, $\Delta k_{\perp}$, are marked in the figure as well. The resulting stationary value $\Delta k_{\perp}\approx 1.111a^{-1}$, where a denotes the fcc lattice parameter, yields oscillations with a period $\Lambda=2\pi/\Delta k_{\perp}\approx 11.3$ ML, in a very good agreement with the period observed in the calculated data, see bottom panel of Fig. 1. The large amplitudes of the oscillations can qualitatively be understood in terms of the small curvatures of the two FS sheets at the stationary point.[55]

The FS origin of the oscillations of $C_{\mathcal{L}}^{\mathrm{mix}}$ in the pure Cu/Ni/Cu(100) system can be documented by their sensitivity with respect to alloying in the magnetic film. The thickness dependence of $C_{\mathcal{L}}^{\mathrm{mix}}$ for the Cu/Py/Cu(100) system (where Py denotes a random fcc $Ni_{0.84}Fe_{0.16}$ alloy) is free of any long-range oscillations, see bottom panel of Fig. 1. The randomly placed Fe impurities are very efficient in suppressing the quantum interference effects in the Ni films and the asymptotic values of the spin-mixing conductance are obtained already for Py film thickness of about 12 ML.

Since effects of alloying on FS properties can be very different in different parts of the alloy BZ[61] and, for FM alloys, in the two spin channels,[59,62] we present the spin-resolved Bloch spectral functions (BSFs) of the fcc $Ni_{0.84}Fe_{0.16}$ alloy in Fig. 3. The BSFs are evaluated for the $\mathbf{k}$ point in the center of the Γ-K line, i.e., close to the stationary point relevant for the oscillations of $C_{\mathcal{L}}^{\mathrm{mix}}$ in the pure

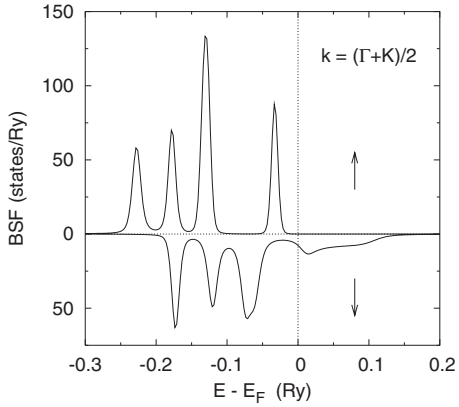

FIG. 3. The spin-polarized Bloch spectral functions of the random fcc $Ni_{0.84}Fe_{0.16}$ alloy as functions of energy E for a $\mathbf{k}$ point in the center of the Γ-K line of the BZ.

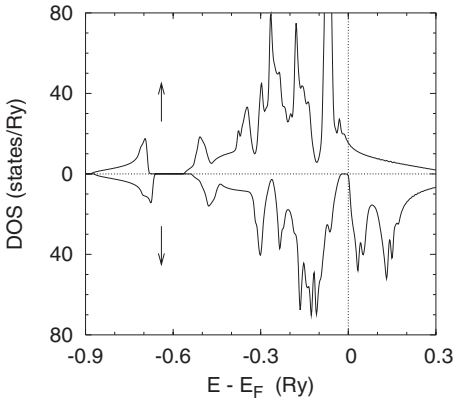

FIG. 4. Spin-polarized densities of states (per formula unit) of the Heusler compound Co_2MnSi as functions of energy E.

Cu/Ni/Cu(100) system, see Fig. 2. The spectral function for majority electrons near the alloy Fermi energy is characterized by a narrow Lorentzian peak indicating a weak alloy disorder whereas a broad non-Lorentzian shape is observed in the minority channel slightly above the Fermi level. This broad peak is closely related to a virtual Fe d bound state located in the same energy range in the minority density of states (DOS) of Ni-rich fcc NiFe alloys;[62] the latter features prove a strong scattering regime which is responsible for the absence of oscillations of $C_{\mathcal{L}}^{\mathrm{mix}}$ in the Cu/Py/Cu(100) system.

B. Films of the Heusler compound Co_2MnSi

The ferromagnetic full-Heusler compound Co_2MnSi with an $L2_1$ structure represents an interesting system for spintronics due to its high Curie temperature of 985 K (Ref. 63) and due to its half-metallicity that was predicted theoretically a few years ago[64,65] and that has very recently been confirmed experimentally.[66]

The $L2_1$ structure consists of four interpenetrating fcc sublattices with origins shifted to points (0,0,0), $(a/4,a/4,a/4)$, $(a/2,a/2,a/2)$, and $(3a/4,3a/4,3a/4)$, where a denotes the fcc lattice parameter. In the case of the Co_2MnSi compound, these four sublattices are consecutively occupied by Co, Mn, Co, and Si atoms. The bulk self-consistent spin-polarized DOSs of the compound, calculated by means of the TB-LMTO method for an experimental fcc lattice (a=0.565 nm),[63] are presented in Fig. 4. The minority-spin DOS is characterized by a narrow band gap that is 0.43 eV wide and by the Fermi energy E_F located only 0.05 eV below the bottom of the conduction band, in reasonable agreement with the experiment providing the width of the band gap of 0.35–0.40 eV and a very small energy separation of 0.01 eV between the E_F and the conduction band.[66] The calculated total spin moment of $5\mu_B$ per formula unit as well as the final DOS shapes agree well with existing full-potential results.[65]

The CPP transport properties are studied for (100) films of the Co_2MnSi compound embedded between nonmagnetic bcc Cr(100) leads, as motivated by prepared Cr/Co_2MnSi epitaxial interfaces.[66] All atoms are located at sites of an ideal bcc lattice leading thus to a small ($\sim$2%) compression inside the Cr electrodes as compared to an equilibrium Cr bcc lattice parameter. The Co_2MnSi films contain an even number of atomic layers with the pure Co layer and the MnSi layer neighboring the left and the right Cr lead, respectively.

The resulting transport properties versus the Co_2MnSi thickness are plotted in Fig. 5. The spin-resolved conductances (top panel of Fig. 5) correspond to a metallic and a tunneling regime in the two spin channels. The majority conductance is essentially constant with unimportant oscillations due to interference effects whereas the minority conductance

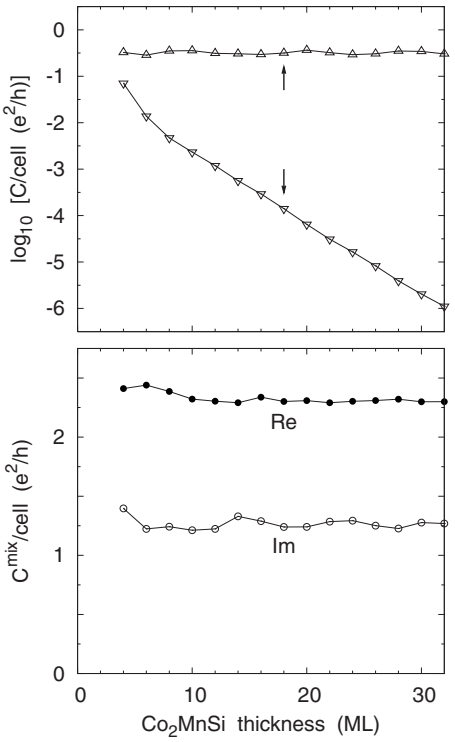

FIG. 5. CPP conductances of Cr/Co_2MnSi/Cr(100) as functions of the Co_2MnSi thickness: spin-resolved conductances on a logarithmic scale for majority (↑) and minority (↓) electrons (top panel) and the real and the imaginary parts of the spin-mixing conductance (bottom panel).

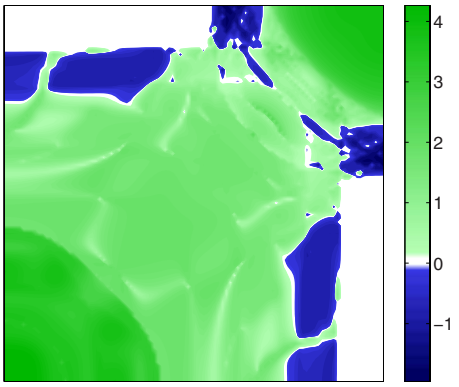

FIG. 6. (Color online) $\mathbf{k}_{\parallel}$-resolved contributions to the imaginary part of the spin-mixing conductance of the system $Cr/Co_2MnSi/Cr(100)$ with a 20 ML thick Co_2MnSi film. The square displays one-quarter of the full 2D BZ and it is equivalent to two irreducible BZs; the $\bar{\Gamma}$ point is located in the lower left corner, the $\bar{M}$ point lies in the upper right corner, and the two remaining corners correspond to the $\bar{X}$ points.

decreases exponentially with increasing film thickness, despite the tiny energy separation between the E_F and the bottom of the bulk minority-spin conduction band.

The thickness dependence of the spin-mixing conductance (bottom panel of Fig. 5) exhibits a nearly constant value with superimposed small oscillations due to quantum-size effects, in analogy to the case of metallic FM films with a strong exchange splitting, e.g., Cu/Co/Cu(111) and Au/Fe/Au(100);[17,21] the real part of $C_{\mathcal{L}}^{\mathrm{mix}}$ has values only slightly smaller than the Sharvin conductance of the bcc Cr(100) lead, $C_{Sh}=2.63e^2/h$ (per one spin and two interface Cr atoms). However, the imaginary part of $C_{\mathcal{L}}^{\mathrm{mix}}$ acquires values as high as one-half of the real part in the case of $Cr/Co_2MnSi/Cr(100)$. Such a high value of the imaginary part of the spin-mixing conductance has not been encountered in metallic NM/FM and NM/FM/NM systems;[17,18,21] this new feature deserves thus a more detailed study.

The $\mathbf{k}_{\parallel}$-resolved contributions to the total imaginary part of the $C_{\mathcal{L}}^{\mathrm{mix}}$ are shown in Fig. 6 for a 20 ML thick film of Co_2MnSi. Note that due to the $L2_1$ structure of the film, the 2D BZ of the $Cr/Co_2MnSi/Cr(100)$ system forms only one-half of the 2D BZ corresponding to the 1×1 unit cell of the bcc Cr(100) electrode; moreover, the two BZs were rotated mutually by 45° for computational reasons. One can see that dominating positive contributions originate in regions around the $\bar{\Gamma}$ and $\bar{M}$ points; regions close to the $\bar{X}$ points are characterized by parts of the 2D BZ without propagating channels in the Cr leads[17] surrounded by small areas with slightly negative contributions. The rest of the $\mathbf{k}_{\parallel}$ points yield positive contributions of minor magnitudes. The sum of the negative $\mathbf{k}_{\parallel}$-resolved contributions amounts only to 7% of the total Im $C_{\mathcal{L}}^{\mathrm{mix}}$. These facts distinguish the present system with a half-metallic ferromagnet from the studied metallic systems[18,21] where significant cancellation of positive and negative contributions takes place that results in a small net total sum. The reduced destructive interference in the $Cr/Co_2MnSi/Cr(100)$ system is explained qualitatively in Sec. IV D.

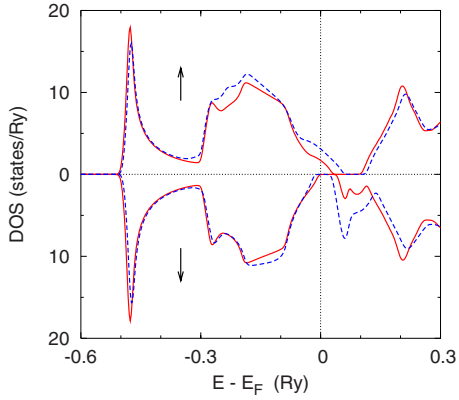

FIG. 7. (Color online) Spin-polarized densities of states (per formula unit) of the bulk diluted $(Ga_{1-x}Mn_x)As$ ferromagnetic semiconductor as functions of energy E: for $x=0.03$ (full red curves) and $x=0.10$ (dashed blue curves).

C. Films of (Ga,Mn)As diluted magnetic semiconductor

The diluted ferromagnetic semiconductors, such as Mn-doped GaAs,[67,68] represent systems with full spin polarization of electron states at the Fermi energy and a small average exchange splitting; this particular combination of spin-dependent properties might lead to unexpected CPP transport characteristics including the spin-mixing conductance.

The bulk electronic structure obtained within the LSDA for the $Ga_{1-x}Mn_xAs$ alloy using the TB-LMTO-CPA technique is shown in Fig. 7 in terms of spin-polarized DOSs. The computational treatment of the system relies on the same four fcc sublattices as in Sec. IV B with consecutive occupancies by the atomic species as follows: $Ga_{1-x}Mn_x$, As, Vac_1, and Vac_2, where the latter two symbols denote so-called empty atomic spheres introduced for reasons of good space filling. The experimental fcc lattice parameter ($a=0.565$ nm) of the parent GaAs semiconductor is used throughout the whole interval of Mn concentration studied ($0.03\leqslant x\leqslant 0.10$). Further details on the bulk electronic structures can be found in Refs. 69 and 70. The resulting DOSs exhibit clear half-metallic features with the Fermi energy inside the minority-spin band gap; the separation between the E_F and the top of the minority-spin valence band is appreciably smaller as compared to the width of the minority-spin band gap as well as to the width of the unoccupied part of the majority-spin valence band (see Fig. 7).

For examination of the CPP transport properties of the (Ga,Mn)As alloy, its films in (100) stacking direction are chosen and attached to bcc Cr(100) electrodes, motivated by the small lattice mismatch between the two systems. The ideal bcc structure used for these systems corresponds again to a 2% compression of the bcc Cr lattice; the (Ga,Mn)As films contain an odd number of atomic layers, terminated on both sides by As layers.

The spin-resolved CPP conductances of the $Cr/(Ga,Mn)As/Cr(100)$ systems exhibit a tunneling regime for the minority-spin channel due to the half-metallic nature of the bulk (Ga,Mn)As, whereas an Ohmic regime is encountered in the majority-spin channel for film thicknesses bigger

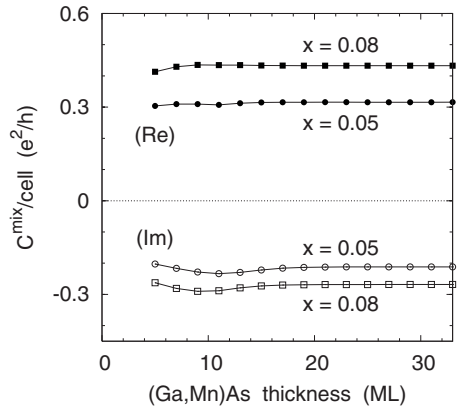

FIG. 8. The spin-mixing conductances of $Cr/(Ga_{1-x}Mn_x)As/Cr(100)$ for $x=0.05$ and $x=0.08$ as functions of the (Ga,Mn)As thickness: the real part (full symbols) and the imaginary part (empty symbols).

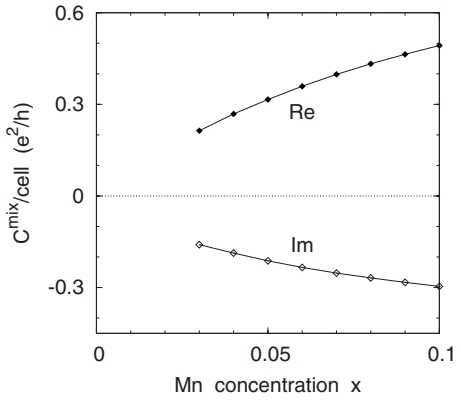

FIG. 9. Concentration dependence of the spin-mixing conductance of $Cr/(Ga_{1-x}Mn_x)As/Cr(100)$ for a fixed (Ga,Mn)As thickness of 21 ML: the real part (full symbols) and the imaginary part (empty symbols).

than 15 ML.[30] The latter fact proves a very strong intrinsic disorder in the (Ga,Mn)As films despite the small content of Mn impurities.

The dependences of the spin-mixing conductance on the (Ga,Mn)As thickness are presented in Fig. 8 for two Mn concentrations. Similar dependences have been found for all other concentrations; they reveal rapid convergence of $C_{\mathcal{L}}^{\mathrm{mix}}$ with increasing film thickness. The magnitude of the imaginary part is again comparable to the real part as in the case of the Co_2MnSi films. There are, however, two striking differences between the two half-metallic systems: the signs of Im $C_{\mathcal{L}}^{\mathrm{mix}}$ are different, and the magnitudes of $C_{\mathcal{L}}^{\mathrm{mix}}$ are significantly smaller in the (Ga,Mn)As case than in the Co_2MnSi case, see Figs. 5 and 8. Note that small spin-mixing conductances with comparable magnitudes of real and imaginary parts were reported for interfaces of doped nonmagnetic semiconductors (InAs) and metallic ferromagnets (Fe),[71] which has been explained by a very small FS of the doped semiconductor.[17]

In order to get understanding of the present results, asymptotic values of the spin-mixing conductance, obtained for a large fixed (Ga,Mn)As thickness, are plotted in Fig. 9 as functions of the Mn content x. One can see that both the real and the imaginary parts exhibit simple concentration trends, namely, their magnitudes increase monotonically with increasing x. These trends indicate that an origin of the small values of $C_{\mathcal{L}}^{\mathrm{mix}}$ might be closely related to the number of holes in the majority-spin valence band of the bulk (Ga,Mn)As, see Fig. 7, or, equivalently, to its majority FS.[72] This interpretation is also supported by a quantitative analysis of a simple free-electron model carried out in the next section.

D. Free-electron model

The results obtained in Secs. IV B and IV C for spin-mixing conductances in the presence of qualitatively different half-metallic FM films deserve a unifying theoretical picture capable to explain roughly the reported properties. For this reason, we consider here a very simple free-electron model of the NM/FM/NM system that has been frequently quoted in the literature, mainly in a context of metallic systems.[13,21]

Since the minority-spin channel is in a tunneling regime both for Co_2MnSi and (Ga,Mn)As films, the contribution of transmitted electrons, $C_{\mathcal{L}}^{\mathcal{R},\mathrm{mix}}$ in Eq. (27), becomes negligible for thicker films and the problem can thus be reduced to the contribution of reflected electrons, $C_{\mathcal{L}}^{\mathcal{L},\mathrm{mix}}$ in Eq. (27), evaluated for a single NM/FM interface of two semi-infinite parts.

Let us denote the spin-resolved values of the constant potential in the FM half-metal as U_s $(s=\uparrow,\downarrow)$, while the constant potential inside the NM metal is set zero, i.e., it is taken as a reference value for one-electron energies. The minority-spin potential is always repulsive, $U_\downarrow>0$, whereas both signs of the majority-spin potential $U_\uparrow$ are allowed in the range $U_\uparrow<U_\downarrow$. The reflection coefficients obtained at a NM/FM interface in a 1D system (Sec. II C) for electrons with a kinetic energy $E>0$ in the NM metal are given by

$$r_s(E)=\frac{1}{U_s}[2E-U_s-2\sqrt{E(E-U_s)}],\quad s=\uparrow,\downarrow, \tag{37}$$

where $\sqrt{E(E-U_s)}\equiv i\sqrt{E(U_s-E)}$ has to be used for $E<U_s$.

The electron energy at the studied NM/FM interface contains a kinetic contribution due to the electron motion in two directions parallel to the interface; this leads to a variation of the energy E of the perpendicular motion in the range $0\leqslant E\leqslant E_F$ where the positive Fermi energy E_F represents another parameter of the model. The latter is further constrained by $E_F\leqslant U_\downarrow$ owing to the assumed half-metallicity of the FM part. Integration of $C_{\mathcal{L}}^{\mathcal{L},\mathrm{mix}}$, Eq. (35), over the $\mathbf{k}_\parallel$ vectors yields the resulting spin-mixing conductance in a form

$$\frac{C_{\mathcal{L}}^{\mathrm{mix}}}{C_{Sh}}=\frac{1}{E_F}\int_0^{E_F}[1-r_\uparrow(E)r_\downarrow^*(E)]dE, \tag{38}$$

where C_{Sh} denotes the Sharvin conductance of the NM metal per one spin channel.

In order to make the model appropriate for the Cr/Co_2MnSi MnSi system (Sec. IV B), we identify the bottom of the minority-spin band with the Fermi energy, $U_\downarrow$

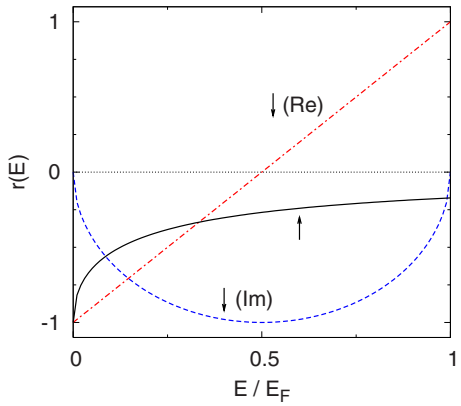

FIG. 10. (Color online) Spin-resolved reflection coefficients in the free-electron model as functions of energy E: in the spin-↑ channel for the potential $U_\uparrow = -E_F$ (black curve) and in the spin-↓ channel for the potential $U_\downarrow = E_F$ (red line, real part; blue curve, imaginary part).

$\equiv E_F$, see Fig. 4, and treat the attractive majority-spin potential $U_\uparrow < 0$ as an independent variable. The model is applicable to the Cr/(Ga,Mn)As system as well; however, one has to take into account the negative effective electron mass at the top of the valence band of bulk (Ga,Mn)As, i.e., a particle-hole symmetry of transport properties must be employed in this case. The restriction to $U_\downarrow \equiv E_F$ can again be used, see Fig. 7, while the majority-spin potential acquires now positive values with the limit $U_\uparrow \to E_F$ corresponding naturally to $x \to 0$ (undoped GaAs).

The reflection coefficients, Eq. (37), in the case of $U_\uparrow < 0$ (Cr/Co_2MnSi), shown in Fig. 10 for a particular negative value of $U_\uparrow$, are real in the majority channel and complex in the minority channel. Consequently, they do not lead to any destructive interference effects in the Im $C_{\mathcal{L}}^{\mathrm{mix}}$, Eq. (38), and the latter can reach positive values non-negligible with respect to the Re $C_{\mathcal{L}}^{\mathrm{mix}}$, see Fig. 11, in qualitative agreement with data in the bottom panel of Fig. 5. Note that $C_{\mathcal{L}}^{\mathrm{mix}}/C_{Sh} \to 1 + i\pi/4$ for $U_\uparrow \to -\infty$, hence Im $C_{\mathcal{L}}^{\mathrm{mix}}$ can be as high as 78% of Re $C_{\mathcal{L}}^{\mathrm{mix}}$ in the present model. Moreover, the real part of $C_{\mathcal{L}}^{\mathrm{mix}}$ comes out slightly smaller than the Sharvin

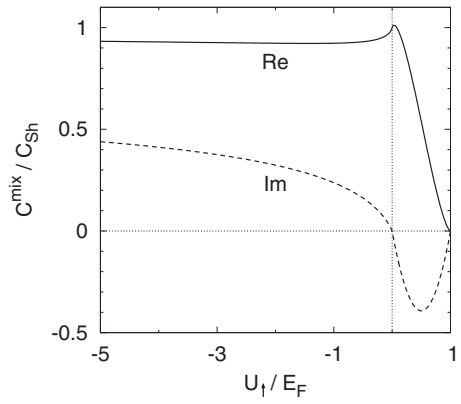

FIG. 11. The spin-mixing conductance in the free-electron model as a function of the majority-spin potential $U_\uparrow$ (full curve, real part; dashed curve, imaginary part).

conductance of the NM metal, see Fig. 11, reproducing thus another feature of the results of Sec. IV B.

The case of positive $U_\uparrow$ (Cr/(Ga,Mn)As) leads to complex reflection coefficients in both spin channels. In the limit of $U_\uparrow \to E_F$ (diluted case, $x \to 0$), the spin-mixing conductance tends to zero, the magnitudes of the Re $C_{\mathcal{L}}^{\mathrm{mix}}$ and the Im $C_{\mathcal{L}}^{\mathrm{mix}}$ become comparable, and the sign of the latter is negative, see Fig. 11. The magnitudes, signs, and concentration trends of the data points in Fig. 9 are thus semiquantitatively explained by the adopted simple free-electron model.

V. CONCLUSIONS

We have developed a nonequilibrium Green's-function approach to the linear response of the spin torque and the spin fluxes at a ferromagnetic thin film due to the spin accumulation in one of adjacent nonmagnetic electrodes. We have sketched an equivalence of the developed scheme to the standard Landauer (scattering theory) formulation of the spin-mixing conductance and have given a proof of invariance of the response coefficients with respect to the choice of boundaries between the semi-infinite leads and the intermediate region. The theory was implemented on an *ab initio* level using the TB-LMTO method; application to several examples yields results that partly disprove general conclusions drawn from previous studies of other systems.

In contrast to metallic ferromagnets with a large exchange splitting (Fe, Co) where strong damping of the transverse spin current takes place, the weak splitting of nickel and the particular shape of its Fermi surfaces are responsible for pronounced long-range oscillations of the calculated spin-mixing conductance of Cu/Ni/Cu(100) system as a function of the film thickness. The period of the oscillations can be quantitatively described by existing theories. This oscillatory behavior proves that the transverse component of the spin current in the nickel film is not absorbed within a few atomic layers near the interface but it survives over appreciably longer distances.

Half-metallic ferromagnetic films exhibit spin-mixing conductances with magnitudes of the imaginary parts comparable to the real parts; this has been demonstrated both for a strongly polarized system, namely, the full-Heusler compound Co_2MnSi, and for diluted ferromagnetic semiconductors (Ga,Mn)As. This property as well as other features of the spin-mixing conductance (magnitude, sign of the imaginary part, concentration dependence) have been explained within a free-electron model of the spin-polarized metal/half-metal interface. The non-negligible imaginary part of the spin-mixing conductance can give rise to big perpendicular (out-of-plane) spin-transfer torques in spin valves containing half-metallic ferromagnetic layers. The obtained results can also be important for studies of magnetization dynamics of thin films in contact with nonmagnetic electrodes, since the imaginary part of the spin-mixing conductance is directly related to the effective gyromagnetic ratio entering the Landau-Lifshitz-Gilbert equation of motion as discussed in Refs. 21, 35, and 39.

The present Green's-function formulation of the linear response is inevitable for application of effective-medium

theories of substitutional disorder, such as the coherent potential approximation, and it will be used in future systematic investigations, e.g., of effects of interdiffusion at the Cu/Ni interface or of antisite atoms in the half-metallic ferromagnetic compounds and diluted ferromagnetic semiconductors.

ACKNOWLEDGMENTS

The authors acknowledge the financial support provided by the Ministry of Education of the Czech Republic (No. MSM0021620834), the Academy of Sciences of the Czech Republic (No. AV0Z20410507, No. KAN400100653), and the Grant Agency of the Academy of Sciences of the Czech Republic (No. A100100616).

APPENDIX: INVARIANCE PROPERTY OF THE SPIN-MIXING CONDUCTANCE

Let us consider the thermodynamic average of a one-particle quantity Q (e.g., a component of the spin torque or of the spin current) in a stationary nonequilibrium state,

$$\bar{Q} = \frac{1}{2\pi}\int_{-\infty}^{\infty} \mathrm{Tr}\{QG^r(E)\Sigma^<(E)G^a(E)\}dE, \tag{A1}$$

where Q is an operator nonzero only inside the intermediate region, denoted here by $\mathcal{I}$, the trace refers to the Hilbert space of $\mathcal{I}$ and the self-energy $\Sigma^<(E)$ is given by Eqs. (10) and (11). In contrast to the usual case of scalar Fermi-Dirac functions $f_{\mathcal{L},\mathcal{R}}(E)$, the presence of spin accumulation in the leads requires to include spin-dependent distributions. This means that $f_{\mathcal{L},\mathcal{R}}(E)$ in Eq. (11) must be understood as operators acting only on spin indices; for a given lead $(\mathcal{L},\mathcal{R})$ and a given energy E, this operator is uniquely specified by a Hermitian 2×2 matrix. We assume that $f_{\mathcal{L}}(E)$ commutes with the Hamiltonian H inside the left lead, so that $[f_{\mathcal{L}}(E),\Sigma^{r,a}_{\mathcal{L}}(E)]=0$, and similarly for the right lead; however, the operators $f_{\mathcal{L},\mathcal{R}}(E)$ do not in general commute with H inside the intermediate region $\mathcal{I}$ and with the operator Q. Let us prove that the resulting $\bar{Q}$, Eq. (A1), does not depend on positions of interfaces $\mathcal{L}/\mathcal{I}$ and $\mathcal{I}/\mathcal{R}$ (provided that Q remains localized in $\mathcal{I}$). It is implicitly assumed that matrix elements of H are short ranged, i.e., H is a tight-binding Hamiltonian.

The total value $\bar{Q}$ can easily be decomposed in two contributions according to Eqs. (10) and (11), $\bar{Q}=\bar{Q}_{\mathcal{L}}+\bar{Q}_{\mathcal{R}}$, where

$$\bar{Q}_{\mathcal{L},\mathcal{R}} = \frac{1}{2\pi}\int_{-\infty}^{\infty} \mathrm{Tr}\{QG^r(E)f_{\mathcal{L},\mathcal{R}}(E)\Gamma_{\mathcal{L},\mathcal{R}}(E)G^a(E)\}dE. \tag{A2}$$

Since the propagators $G^{r,a}(E)$ refer to the whole infinite system while the operator Q is localized in the interior of $\mathcal{I}$ and the operators $\Gamma_{\mathcal{L},\mathcal{R}}$ are localized in narrow regions at the respective interfaces, it is obvious that the contribution $\bar{Q}_{\mathcal{R}}$ does not depend on the position of the $\mathcal{L}/\mathcal{I}$ interface and vice versa.

Let us investigate the dependence, e.g., of $\bar{Q}_{\mathcal{L}}$, on the position of the $\mathcal{L}/\mathcal{I}$ interface. Let us move the interface toward the left, which results in a modified lead $\tilde{\mathcal{L}}\subset\mathcal{L}$ and a region Λ of a finite thickness such that $\Lambda=\mathcal{L}\backslash\tilde{\mathcal{L}}$, $\mathcal{L}=\tilde{\mathcal{L}}\cup\Lambda$. The original intermediate region $\mathcal{I}$ is thus modified to an extended region $\tilde{\mathcal{I}}=\Lambda\cup\mathcal{I}$. An explicit expression of $\bar{Q}_{\mathcal{L}}$, Eq. (A2), in terms of the left self-energies is given by

$$\bar{Q}_{\mathcal{L}} = \frac{i}{2\pi}\int_{-\infty}^{\infty} \mathrm{Tr}\{QG^r(E)f_{\mathcal{L}}(E)[\Sigma^r_{\mathcal{L}}(E)-\Sigma^a_{\mathcal{L}}(E)]G^a(E)\}dE, \tag{A3}$$

where the trace refers to the original intermediate region $\mathcal{I}$.

Let us consider the original lead $\mathcal{L}$ decoupled from the rest of the system; its Green's function projected on the region Λ will be denoted $\mathcal{G}^{r,a}_{\mathcal{L}}(E)$. It holds $[f_{\mathcal{L}}(E),\mathcal{G}^{r,a}_{\mathcal{L}}(E)]=0$. The self-energy of the original left lead can be expressed as

$$\Sigma^{r,a}_{\mathcal{L}}(E) = t\mathcal{G}^{r,a}_{\mathcal{L}}(E)t^\dagger, \tag{A4}$$

where t denotes that part of the Hamiltonian H that describes hoppings from Λ to $\mathcal{I}$ while $t^\dagger$ describes hoppings from $\mathcal{I}$ to Λ; these (spin-independent) hoppings satisfy $[f_{\mathcal{L}}(E),t]=0$. We assume for simplicity that Λ is thick enough so that no matrix elements of H couple $\tilde{\mathcal{L}}$ to $\mathcal{I}$. Substitution of Eq. (A4) in Eq. (A3) yields

$$\bar{Q}_{\mathcal{L}} = \frac{i}{2\pi}\int_{-\infty}^{\infty} \mathrm{Tr}\{QG^r(E)tf_{\mathcal{L}}(E)[\mathcal{G}^r_{\mathcal{L}}(E)-\mathcal{G}^a_{\mathcal{L}}(E)]t^\dagger G^a(E)\}dE. \tag{A5}$$

Let us further denote by $\tilde{\Sigma}^{r,a}_{\mathcal{L}}(E)$ the self-energy of the modified lead $\tilde{\mathcal{L}}$. Since $\mathcal{G}^{r,a}_{\mathcal{L}}(E)$ refers to the Green's function of $\mathcal{L}=\tilde{\mathcal{L}}\cup\Lambda$, i.e., of a finite region Λ attached to the semi-infinite lead $\tilde{\mathcal{L}}$, the following relation holds:

$$\mathcal{G}^r_{\mathcal{L}}(E)-\mathcal{G}^a_{\mathcal{L}}(E) = \mathcal{G}^r_{\mathcal{L}}(E)[\tilde{\Sigma}^r_{\mathcal{L}}(E)-\tilde{\Sigma}^a_{\mathcal{L}}(E)]\mathcal{G}^a_{\mathcal{L}}(E), \tag{A6}$$

which represents an analogy to Eqs. (9) and (19). The use of Eq. (A6) in Eq. (A5) leads to

$$\bar{Q}_{\mathcal{L}} = \frac{i}{2\pi}\int_{-\infty}^{\infty} \mathrm{Tr}\{QG^r(E)t\mathcal{G}^r_{\mathcal{L}}(E)f_{\mathcal{L}}(E)[\tilde{\Sigma}^r_{\mathcal{L}}(E) - \tilde{\Sigma}^a_{\mathcal{L}}(E)]\mathcal{G}^a_{\mathcal{L}}(E)t^\dagger G^a(E)\}dE. \tag{A7}$$

Finally, let us take into account the Dyson equation for a coupling of the isolated left lead $\mathcal{L}=\tilde{\mathcal{L}}\cup\Lambda$ to the rest of the whole system, $\mathcal{I}\cup\mathcal{R}$, by using the hoppings t and $t^\dagger$ as a perturbation. Since the operator Q is localized inside the region $\mathcal{I}$ while the self-energy $\tilde{\Sigma}^{r,a}_{\mathcal{L}}(E)$ is localized in Λ, one can replace the products $G^r(E)t\mathcal{G}^r_{\mathcal{L}}(E)$ and $\mathcal{G}^a_{\mathcal{L}}(E)t^\dagger G^a(E)$ in Eq. (A7) by the perturbed Green's functions $\tilde{G}^r(E)$ and $\tilde{G}^a(E)$, respectively. Here, the $\tilde{G}^{r,a}(E)$ denote propagators of the coupled infinite system, projected on the extended intermediate region $\tilde{\mathcal{I}}$, in contrast to their projections $G^{r,a}(E)$ on the original region $\mathcal{I}$. This replacement yields a modified formula for $\bar{Q}_{\mathcal{L}}$,

$$\bar{Q}_{\mathcal{L}} = \frac{i}{2\pi}\int_{-\infty}^{\infty} \mathrm{Tr}\{Q\tilde{G}^r(E)f_{\mathcal{L}}(E)[\tilde{\Sigma}^r_{\mathcal{L}}(E) - \tilde{\Sigma}^a_{\mathcal{L}}(E)]\tilde{G}^a(E)\}dE, \tag{A8}$$

where the trace is taken over the extended region $\tilde{\mathcal{I}}$. A comparison of Eq. (A8) and Eq. (A3) proves insensitivity of the contribution $\bar{Q}_{\mathcal{L}}$ to the position of the $\mathcal{L}/\mathcal{I}$ interface. This completes a proof of the invariance of the thermodynamic average $\bar{Q}$, Eq. (A1), with respect to the $\mathcal{L}/\mathcal{I}/\mathcal{R}$ partitioning.

The same invariance holds for the spin-mixing conductance $C^{\mathrm{mix}}_{\mathcal{L}}$, Eq. (21), as well as for other quantities, Eqs. (27) and (28), that can be obtained by infinitesimal variations of averages of the form (A1).

*carva@karlov.mff.cuni.cz
†turek@ipm.cz

[1] *Spin Dependent Transport in Magnetic Nanostructures*, edited by S. Maekawa and T. Shinjo (CRC, Boca Raton, FL, 2002).
[2] *Concepts in Spin Electronics*, edited by S. Maekawa (Oxford University Press, New York, 2006).
[3] J. Bass and W. P. Pratt, Jr., J. Magn. Magn. Mater. **200**, 274 (1999).
[4] J. C. Slonczewski, J. Magn. Magn. Mater. **159**, L1 (1996).
[5] L. Berger, Phys. Rev. B **54**, 9353 (1996).
[6] J. A. Katine, F. J. Albert, R. A. Buhrman, E. B. Myers, and D. C. Ralph, Phys. Rev. Lett. **84**, 3149 (2000).
[7] M. AlHajDarwish, H. Kurt, S. Urazhdin, A. Fert, R. Loloee, W. P. Pratt, Jr., and J. Bass, Phys. Rev. Lett. **93**, 157203 (2004).
[8] D. Chiba, Y. Sato, T. Kita, F. Matsukura, and H. Ohno, Phys. Rev. Lett. **93**, 216602 (2004).
[9] T. Valet and A. Fert, Phys. Rev. B **48**, 7099 (1993).
[10] A. Fert, V. Cros, J.-M. George, J. Grollier, H. Jaffres, A. Hamzic, A. Vaures, G. Faini, J. Ben Youssef, and H. Le Gall, J. Magn. Magn. Mater. **272-276**, 1706 (2004).
[11] J. Barnas, A. Fert, M. Gmitra, I. Weymann, and V. K. Dugaev, Phys. Rev. B **72**, 024426 (2005).
[12] J. Barnas, A. Fert, M. Gmitra, I. Weymann, and V. K. Dugaev, Mater. Sci. Eng., B **126**, 271 (2006).
[13] M. D. Stiles and A. Zangwill, Phys. Rev. B **66**, 014407 (2002).
[14] J. C. Slonczewski, J. Magn. Magn. Mater. **247**, 324 (2002).
[15] A. Brataas, Y. V. Nazarov, and G. E. W. Bauer, Phys. Rev. Lett. **84**, 2481 (2000).
[16] A. Brataas, Y. V. Nazarov, and G. E. W. Bauer, Eur. Phys. J. B **22**, 99 (2001).
[17] A. Brataas, G. E. W. Bauer, and P. J. Kelly, Phys. Rep. **427**, 157 (2006).
[18] K. Xia, P. J. Kelly, G. E. W. Bauer, A. Brataas, and I. Turek, Phys. Rev. B **65**, 220401(R) (2002).
[19] S. Datta, *Electronic Transport in Mesoscopic Systems* (Cambridge University Press, Cambridge, 1995).
[20] K. Xia, M. Zwierzycki, M. Talanana, P. J. Kelly, and G. E. W. Bauer, Phys. Rev. B **73**, 064420 (2006).
[21] M. Zwierzycki, Y. Tserkovnyak, P. J. Kelly, A. Brataas, and G. E. W. Bauer, Phys. Rev. B **71**, 064420 (2005).
[22] A. A. Kovalev, G. E. W. Bauer, and A. Brataas, Phys. Rev. B **73**, 054407 (2006).
[23] D. Huertas-Hernando and Y. V. Nazarov, Eur. Phys. J. B **44**, 373 (2005).
[24] H. Haug and A.-P. Jauho, *Quantum Kinetics in Transport and Optics of Semiconductors* (Springer, Berlin, 1996).
[25] O. K. Andersen and O. Jepsen, Phys. Rev. Lett. **53**, 2571 (1984).
[26] I. Turek, V. Drchal, J. Kudrnovský, M. Šob, and P. Weinberger, *Electronic Structure of Disordered Alloys, Surfaces and Interfaces* (Kluwer, Boston, 1997).
[27] P. Soven, Phys. Rev. **156**, 809 (1967).
[28] B. Velický, Phys. Rev. **184**, 614 (1969).
[29] J. Kudrnovský and V. Drchal, Phys. Rev. B **41**, 7515 (1990).
[30] K. Carva, I. Turek, J. Kudrnovský, and O. Bengone, Phys. Rev. B **73**, 144421 (2006).
[31] X. Waintal, E. B. Myers, P. W. Brouwer, and D. C. Ralph, Phys. Rev. B **62**, 12317 (2000).
[32] D. M. Edwards, F. Federici, J. Mathon, and A. Umerski, Phys. Rev. B **71**, 054407 (2005).
[33] A. Kalitsov, I. Theodonis, N. Kioussis, M. Chshiev, W. H. Butler, and A. Vedyayev, J. Appl. Phys. **99**, 08G501 (2006).
[34] S. Datta, J. Phys.: Condens. Matter **2**, 8023 (1990).
[35] Y. Tserkovnyak, A. Brataas, and G. E. W. Bauer, Phys. Rev. B **66**, 224403 (2002).
[36] I. Theodonis, N. Kioussis, A. Kalitsov, M. Chshiev, and W. H. Butler, Phys. Rev. Lett. **97**, 237205 (2006).
[37] K. Capelle, G. Vignale, and B. L. Györffy, Phys. Rev. Lett. **87**, 206403 (2001).
[38] F. Michael and M. D. Johnson, Physica B **339**, 31 (2003).
[39] Y. Tserkovnyak, A. Brataas, and G. E. W. Bauer, Phys. Rev. Lett. **88**, 117601 (2002).
[40] D. S. Fisher and P. A. Lee, Phys. Rev. B **23**, 6851 (1981).
[41] L. Arrachea and M. Moskalets, Phys. Rev. B **74**, 245322 (2006).
[42] P. S. Krstić, X.-G. Zhang, and W. H. Butler, Phys. Rev. B **66**, 205319 (2002).
[43] P. A. Khomyakov, G. Brocks, V. Karpan, M. Zwierzycki, and P. J. Kelly, Phys. Rev. B **72**, 035450 (2005).
[44] I. Turek, J. Kudrnovský, and V. Drchal, in *Electronic Structure and Physical Properties of Solids*, Lecture Notes in Physics, Vol. 535 edited by H. Dreyssé (Springer, Berlin, 2000), p. 349.
[45] J. Kudrnovský, V. Drchal, C. Blaas, P. Weinberger, I. Turek, and P. Bruno, Phys. Rev. B **62**, 15084 (2000).
[46] I. Turek, J. Kudrnovský, V. Drchal, L. Szunyogh, and P. Weinberger, Phys. Rev. B **65**, 125101 (2002).
[47] V. Drchal, J. Kudrnovský, P. Bruno, P. H. Dederichs, I. Turek, and P. Weinberger, Phys. Rev. B **65**, 214414 (2002).
[48] S. V. Faleev, F. Léonard, D. A. Stewart, and M. van Schilfgaarde, Phys. Rev. B **71**, 195422 (2005).
[49] U. von Barth and L. Hedin, J. Phys. C **5**, 1629 (1972).
[50] P. Hohenberg and W. Kohn, Phys. Rev. **136**, B864 (1964).
[51] S. H. Vosko, L. Wilk, and M. Nusair, Can. J. Phys. **58**, 1200 (1980).
[52] Y. Li, S. X. Wang, G. Khanna, and B. M. Clemens, Thin Solid Films **381**, 160 (2001).
[53] K. M. Schep, P. J. Kelly, and G. E. W. Bauer, Phys. Rev. Lett. **74**, 586 (1995).

[54] S. Sanvito, C. J. Lambert, J. H. Jefferson, and A. M. Bratkovsky, Phys. Rev. B **59**, 11936 (1999).
[55] J. Mathon, M. Villeret, and H. Itoh, Phys. Rev. B **52**, R6983 (1995).
[56] J. Mathon, A. Umerski, and M. Villeret, Phys. Rev. B **55**, 14378 (1997).
[57] P. Bruno and C. Chappert, Phys. Rev. Lett. **67**, 1602 (1991).
[58] P. Bruno, Phys. Rev. B **52**, 411 (1995).
[59] I. Mertig, Rep. Prog. Phys. **62**, 237 (1999).
[60] http://www.physik.tu-dresden.de/~fermisur/
[61] J. S. Faulkner, Prog. Mater. Sci. **27**, 1 (1982).
[62] D. D. Johnson, J. B. Staunton, F. J. Pinski, B. L. Gyorffy, and G. M. Stocks, Mater. Res. Soc. Symp. Proc. **253**, 277 (1992).
[63] *Magnetic Properties of Metals: d-Elements, Alloys and Compounds*, edited by H. P. J. Wijn (Springer, Berlin, 1991).
[64] S. Ishida, S. Fujii, S. Kashiwagi, and S. Asano, J. Phys. Soc. Jpn. **64**, 2152 (1995).
[65] I. Galanakis, P. H. Dederichs, and N. Papanikolaou, Phys. Rev. B **66**, 174429 (2002).
[66] Y. Sakuraba, T. Miyakoshi, M. Oogane, Y. Ando, A. Sakuma, T. Miyazaki, and H. Kubota, Appl. Phys. Lett. **89**, 052508 (2006).
[67] H. Ohno, J. Magn. Magn. Mater. **200**, 110 (1999).
[68] F. Matsukura, H. Ohno, and T. Dietl, in *Handbook of Magnetic Materials*, edited by K. H. J. Buschow (North-Holland, Amsterdam, 2002), Vol. 14, Chap. 1, p. 1.
[69] J. Kudrnovský, I. Turek, V. Drchal, F. Máca, P. Weinberger, and P. Bruno, Phys. Rev. B **69**, 115208 (2004).
[70] I. Turek, J. Kudrnovský, V. Drchal, and P. Weinberger, J. Phys.: Condens. Matter **16**, S5607 (2004).
[71] G. E. W. Bauer, A. Brataas, Y. Tserkovnyak, B. I. Halperin, M. Zwierzycki, and P. J. Kelly, Phys. Rev. Lett. **92**, 126601 (2004).
[72] L. Bergqvist, O. Eriksson, J. Kudrnovský, V. Drchal, A. Bergman, L. Nordström, and I. Turek, Phys. Rev. B **72**, 195210 (2005).